C. T.-C. Nguyen, "RF MEMS for Channelizing Low-Power Radios," the 17th Int. Conf. on Solid-State Sensors, Actuators, & Microsystems (Transducers'13), Barcelona, Spain, June 16-20, 2013, pp. 2455-2460.

RF MEMS FOR CHANNELIZING LOW-POWER RADIOS

Clark T.-C. Nguyen
Berkeley Sensor & Actuator Center, Dept. of EECS
Univ. of California at Berkeley, Berkeley, CA, USA

ABSTRACT

RF MEMS technologies are evaluated with regard to their potential to realize the RF frequency gating function targeted for true software-defined cognitive radios and ultra-low power autonomous sensor network radios. Here, RF channel-selection, as opposed to band selection, is key to substantial increases in call volume with simultaneous reduction in power consumption. The MEMS technologies most conducive to RF channel-selecting front-ends include vibrating micromechanical resonators that exhibit record on-chip *Q*'s at GHz frequencies; resonant switches that provide extremely efficient switched-mode power gain for both transmit and receive paths; and medium-scale integrated micromechanical circuits that implement on/off switchable filter-amplifier banks.

KEYWORDS

Software-defined radio, cognitive radio, sensor network, micromechanical circuit, resonator, resoswitch, quality factor, filter, motional resistance.

INTRODUCTION

MEMS-based devices already play important, in some cases critical, roles in wireless communication devices. Examples of MEMS devices already in wireless systems include piezoelectric FBAR resonators used for front-end duplexer filters in cell phones, high-*Q* capacitive-gap transduced resonators used in low-end timing oscillators that are also used in a myriad of applications beyond wireless [2], and more recently, tunable/switchable capacitors for front-end amplifier-to-antenna impedance matching [3] that help to lower transmit power consumption. But this list only scratches the surface of what is possible. Indeed, if newer MEMS-based devices on the horizon are successful, much bigger advances may soon be on hand that just might catalyze key communication architectural paradigm-shifts needed to address fast-growing demands for advanced communication concepts like true software-defined cognitive radio and ultra-low power radios for autonomous sensor networks.

In particular, recent advances in vibrating RF MEMS technology that yield on-chip resonators with *Q*'s over 40,000 at 3GHz [1] and excellent thermal [4] [5] and aging stability [6] may soon enable selection of individual channels (as opposed to bands of many channels) right at RF, which if possible would then lower analog-to-digital converter (ADC) power consumption to levels where true software-defined radio becomes practical. In such an RF channel-selecting system, resonant switch-based filter-amplifiers (for receive) and power amplifiers (for transmit) that obviate transistor amplifiers, thereby removing much of their noise and current draw, also stand to enable radios with unprecedentedly low power consumption for use in autonomous "set-and-forget" sensor networks.

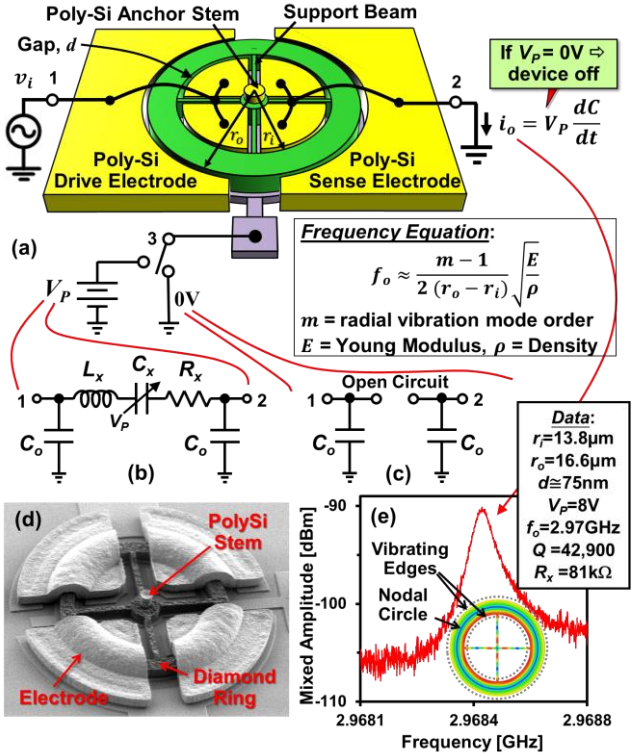

Fig. 1: Summary of the capacitive-gap transduced micromechanical ring resonator. (a) Perspective-view illustration, indicating input port 1 that receives the input sinusoidal voltage, output port 2 from which the output motional current is sensed, and bias port 3 that determines whether the device is (b) "on" when a dc-bias is applied, in which case it behaves as an LCR tank; or (c) "off" when the port is grounded. (d) Scanning electron micrograph (SEM) of a 2.97-GHz μmechanical radial mode ring resonator and (e) measured frequency response with simulated second radial-contour mode shape [1].

Fig. 1 summarizes one recent device—a spoke-supported diamond ring [1]—that actually exhibits enough *Q* for RF channel-selection. This device consists of a 3μm-thick polydiamond ring with 13.8μm and 16.6μm inner and outer radii, respectively, suspended by polysilicon spokes radially emanating from a center stem self-aligned to be exactly at its center, all enclosed by doped polysilicon electrodes spaced less than 80nm from the ring sidewalls. The device can be excited into resonance via a combination of dc and ac voltages, where the presence of the dc voltage governs whether or not the device is "on", in which case it behaves as an *LCR* with shunt C_o terminations, with electromechanical coupling gauged by the ratio (C_x/C_o); or "off", in which case it is a C_o-shunted open circuit [7]. When vibrating in its second contour mode, the ring expands and contracts along its width as shown in Fig. 1(e), in a motion reminiscent of breathing, and at a frequency determined primarily by its width—a lateral CAD-definable dimension that allows realization of rings

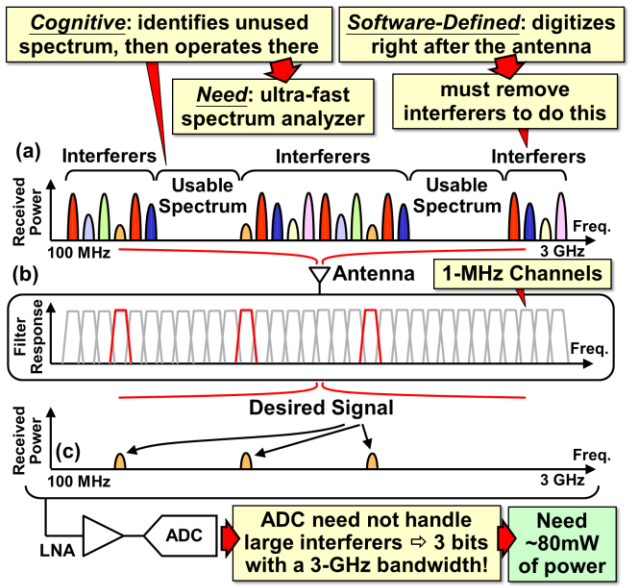

Fig. 2: System block diagram for a software defined radio front-end utilizing a micromechanical RF channel-select filter network to realize a frequency gating function. When one (or more) filters are turned "on", with all others "off", the filter bank realizes a frequency gate. When all filters are turned "on", the bank realizes a real-time spectrum sensor that could be used to assess the entire received spectrum and determine what frequencies might be permissible to operate a cognitive radio. (a) Cartoon of the typical power spectrum that might be received by an antenna-terminated spectrum analyzer atop a tall building at a given moment in time. Here, many channels are unused at this instant, so are available for use by a cognitive radio. (b) On/off configuration of filters in an RF channelizing filter bank that selects specific channels to pass. (c) Output of the filter bank directed to the ADC containing only desired channel signals, and no blockers, allowing substantially lower ADC power consumption.

with many different frequencies in a single thin-film. Quarter-wavelength spoke dimensions and cancellation of (ideally) perfectly balanced forces at the center support greatly suppress anchor losses, allowing this design to attain a record *Q* of 42,000 at 3GHz (*cf.* Fig. 1(e)).

Before expanding on this and other enabling MEMS technologies, it is instructive to first describe next generation wireless communication paradigms and the degree to which they might rely on RF channel-selection.

NEED FOR RF CHANNEL-SELECTION

The increasing desire for reconfigurable radios capable of adapting to any communication standard at any location across the world has spurred great interest in the concept of a software defined radio (SDR) [8], in which the frequencies and modulation schemes of any existing communication standard can be produced in real-time by simply calling up an appropriate software sub-routine. The call volume of such a radio could be substantially increased if it also possessed cognitive abilities, where it might search the frequency spectrum for unused bands using a spectrum analyzer, then operate in an unused band until a priority user wants in, as illustrated in Fig. 2.

As explained more fully in [9], dynamic range considerations dictate that all out-of-channel interferers be removed before the signal received at the antenna is directed to the ADC. Removal of out-of-channel interferers requires filtering much more selective than the 3% bandwidth band-select ones in use today. Rather, as shown in [9], channel-selecting filters with bandwidths on the order of 0.03-0.1% are required to maintain reasonable ADC power consumption. The difference in ADC power consumption with and without such channel-selecting filters is quite substantial. For example, in a GSM-like (i.e., cell phone) blocker environment, a 3-GHz bandwidth ADC with a figure of merit (*FOM*) of 1.83pJ/bit would require 45W of power to process the antenna signal after filtering by a 3% bandwidth filter, but only 80mW after a 0.03% bandwidth channel-select filter [9].

RF channel-selection is beneficial for not only software-defined radio, but any radio, including the ultra-low power receivers needed for sensor networks. As detailed in [10], with all blockers removed, the oscillator phase noise and dynamic ranges of the LNA and mixer in any RF front-end could be relaxed enormously, to the point where highly nonlinear (and thus, low power) designs of these functions might be used. For example, one desirable design might dispense entirely with LNA linearity and just allow the amplifier to rail out, amplifying a tiny sinusoidal FSK input signal to a large square wave FSK signal easily processed by a discriminator, and all with minimal concern for intermodulation or other forms of blocker-generated spurious signals (since there would be no blockers). Merely reducing the quiescent drain current of a conventional LNA should accomplish this, although the degree to which current can be reduced will also depend on the required noise figure.

Programmable Frequency Gate

Whether for SDR or low-power sensor radios, it follows that to eliminate all interferers and pass only the desired signal, a programmable frequency gating device or circuit is needed that can pass and reject tiny (e.g., 0.03% bandwidth) RF frequency channels at will along the entire 3-GHz input frequency span. The need for such small percent bandwidths makes this especially difficult, since the smaller the percent bandwidth, the higher the needed *Q*'s of the resonators comprising a given filter to maintain reasonable insertion loss. For example, the constituent resonators making up a 3-GHz, 0.03% (1MHz) bandwidth, 0.01dB ripple, 4-resonator Chebyshev filter would require *Q*'s >30,000 just to maintain an insertion loss below 3dB [11]. On the upside, smaller filter percent bandwidth requires a smaller, i.e., easier to achieve, electromechanical coupling coefficient. In particular, while the 3% bandwidth filter used in present-day cell phones requires a motional-to-static capacitance ratio (C_x/C_o) of 7% to avoid excessive passband distortion from shunt C_o capacitance, a 0.03% bandwidth filter requires only 0.075%. So going to smaller percent bandwidth does not require in an increase in resonator $(C_x/C_o)\cdot Q$ product, but rather a specific distribution of (C_x/C_o) and *Q*, where the latter increases, perhaps at the expense of the former.

Unfortunately, it is often the case that the higher the *Q* of a resonator, the less tunable it is. In fact, at the time of this writing, there are no existing on-chip resonator technologies capable of achieving *Q*'s >30,000 while also being continuously tunable over a wide span. Fortunately, MEMS technology offers an alternative method to achieve

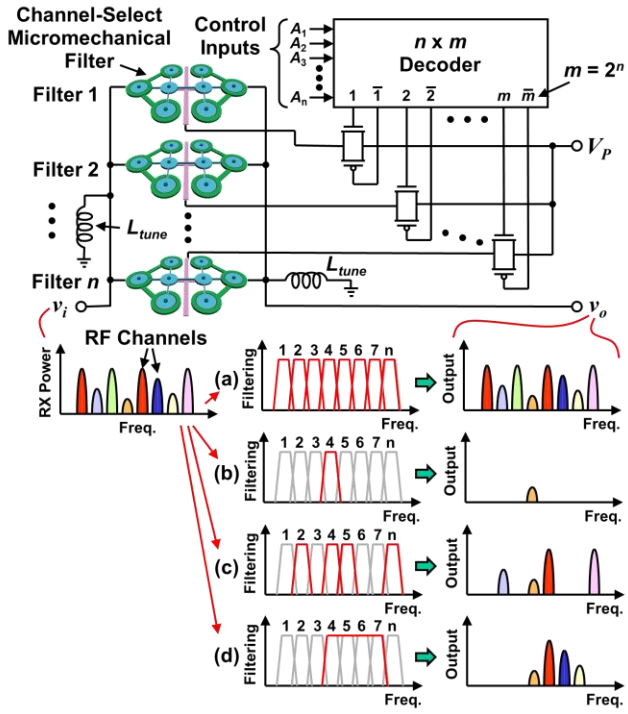

Fig. 3: Schematic of an RF channel-select micromechanical filter bank, with programming examples showing how various input frequencies can be simultaneously selected via mere application or removal of resonator dc-biases. In (a) all filters are on to realize spectrum sensing; (b) only filter 4 is on to select just one channel; (c) filters 2, 4, 5, and n are on to select multiple non-contiguous channels; and (d) adjacent filters 4-7 on and designed to suppress corner-stitched zeros, allowing a contiguous wide bandwidth.

the desired programmable frequency gate that dispenses with the need to tune a given resonator's frequency over a wide range. In particular, being a wafer-level manufacturing technology similar to those used for integrated transistor circuits, MEMS encourages designers to use mechanical devices the same way transistors are used: in massive numbers. So instead of restricting the implementation of a programmable frequency gate to a single tunable filter, MEMS technology allows realization of the same programmable frequency gate via a bank of on/off switchable micromechanical filters, as depicted in Fig. 3, where each filter is realized using an interconnected network of micromechanical resonators, in this case capacitive-gap transduced ones on/off switchable via dc-bias voltages. With RF channel-selecting bandwidths, this might entail thousands of filters, all manageable in wafer-level MEMS technology the same way it is in IC technology, so long as fabrication repeatability is sufficient.

As shown, the circuit of Fig. 3 is capable of not only RF channel-selection, but also with all filters turned on (*cf.* Fig. 3(a)), fast low-power spectrum sensing required by cognitive radio [9]. It also permits simultaneous passage of multiple non-adjacent channels (*cf.* Fig. 3(c)) or passage of larger bandwidths if the individual filters are designed to allow passband corner-stitching (*cf.* Fig. 3(d)). In effect, this bank of tiny bandwidth filters allows real-time configuration into virtually any passband response, be it RF channel-select or not. Thus, it is suitable for virtually any communication standard, including and especially those with variable channel bandwidths, like 4G LTE.

Issue: Shunt Input/Output Capacitance

In the implementation of Fig. 3, where so many filters are placed in parallel, the shunt capacitance at the filter bank input and output nodes can add up to enormous values, making the effective (C_x/C_o) ratio for each filter extremely small. At first glance, this might seem like an enormous problem. Fortunately, if the total shunt capacitance stays constant no matter how many filters are switched in (which is the case for the circuit of Fig. 3), there are some very simple circuits that can eliminate the shunt C_o, including the use of a single low-Q shunt inductor L_{tune} to tune out C_o over a given wide bandwidth, as done in [12]. The larger is the C_o, the smaller the needed L_{tune}, so a larger filter bank might allow the use of an on-chip inductor. Even if the inductor had to be off-chip, this is still an acceptable compromise, given that only two inductors (one for input, one for output) are required for possibly thousands of filters and enormous radio performance enhancement. If a wider band of frequencies over which C_o is negated than possible via a single inductor is needed, then are circuits using more elements that can do this, including matching networks that both null the C_o and impedance transform to match an antenna.

Whichever implementation, this filter bank approach practically removes the need for strong electromechanical coupling, i.e., for large (C_x/C_o), by ironically increasing C_o to the point where at most only two very small inductors are required to tune it out.

HIGH *Q* AND SUFFICIENT COUPLING

Unfortunately, although use of a filter bank with proper tuning obviates the need for strong coupling, sufficient coupling is still desired to reduce the transformer ratio needed for impedance matching to a low impedance antenna. And although capacitive-gap transduced resonators have Qs adequate for RF channel-selection, they lack sufficient electromechanical coupling to present low motional resistance R_x, which relates to electromechanical coupling (C_x/C_o) via the expression $R_x = [\omega_o Q C_o \cdot (C_x/C_o)]^{-1}$ where ω_o is the radian resonance frequency. For example, the device of Fig. 1, with 80nm electrode-to-resonator gaps, posts an abysmal (C_x/C_o) of only 0.000068%, for which array-composites like those used in [12] would need 810 resonators to achieve an effective resonator impedance of 100Ω that for <1dB insertion loss allows a filter termination impedance of 1kΩ, easily transformable to the desired antenna impedance. Needless to say, 810 is a lot of resonators, and this number would need to be multiplied by approximately 3 times the number of filters in the bank.

Piezoelectric resonators, on the other hand, offer plenty of (C_x/C_o). For example, AlN FBARs often exhibit (C_x/C_o) ~7%, and even lateral AlN piezoelectric resonators employing less direct d_{31} coupling can achieve (C_x/C_o) from 1-2% [13]. Unfortunately, none of these piezoelectric resonators share the high Qs of their capacitive-gap counterparts. Rather, they post Qs on the order of 1,000, some higher, but none anywhere near the needed 30,000 for RF channel-selection. Evidently, if piezoelectric resonators are to satisfy the needs of RF channelizers, some method for substantially raising their Qs is required.

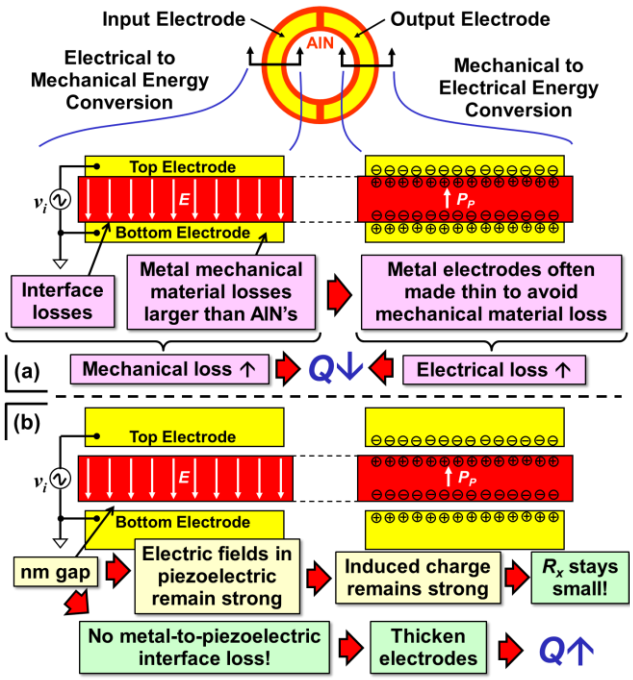

Fig. 4: Comparison of (a) a conventional d_{31} piezoelectric ring resonator, for which metal-to-resonator interface losses, metal electrode material losses, and finite electrode resistance, all contribute to a lower-than-desired Q; and (b) its capacitive-piezo transduced counterpart that alleviates the above issues by merely separating the electrodes from the resonant structure by submicron gaps.

Energy Sharing (or *Q*-Boosting)

One effective method for raising the *Q* of a low-*Q* (piezoelectric) resonator is to energy share it with a higher *Q* resonator. Whether by coupling the low-*Q* resonator via coupling links to other similar resonators, as done in [14], or just combining the piezoelectric material with a higher *Q* material (e.g., silicon, silicon carbide, or diamond) [14] [15], this is a well-known and well-practiced method. This approach has so far achieved *Q*'s as high as 5,510 at 2.92GHz without overmoding [14], and as high as 68,000 at 1.6GHz when employing overmoding using an attached material much thicker than the piezoelectric film [15]. Here, overmoding effectively amplifies the *Q* boost provided by the attached material.

Indeed, it is very encouraging that overmoded *Q*'s can satisfy the needs of RF channel-selection. However, overmoding as done in [15] does have the disadvantages of 1) not being on the micro-scale, so not amenable to massive numbers; and 2) generating not just one passband, but combs of them, the majority of which must be removed by another filter in series at the cost of additional (and very undesirable) insertion loss. It also increases further the complexity of an already complex approach that requires merging of different resonator materials.

To eliminate the need for macro-scale overmoding, the factor by which the *Q* of the piezoelectric resonator is boosted must be lowered, i.e., the starting *Q* of the piezoelectric resonator must be raised.

The Capacitive-Piezoelectric Transducer

As evidenced by the *Q*-boosting experiment of [16], which achieved AlN resonator *Q*'s as high as 10,144 by coupling conventional AlN resonators with electrode-less (and thus, higher *Q*) ones, the key to raising piezoelectric resonator *Q* lies in the recognition that the culprit limiting *Q* in such resonators is often not the piezoelectric resonator, but rather the metal electrode attached to it in conventional designs. Realizing this, [17] circumvents metal losses in a single piezoelectric resonator by merely separating the resonator from its metal electrodes, effectively forming a "capacitive-piezo transducer that combines the isolating advantages of capacitive-gap transduction with the coupling strength of the piezoelectric effect. Fig. 4 summarizes the first such device using the same ring design as in Fig. 1, contrasting it with a conventional piezoelectric resonator (with attached electrode).

Each device in Fig. 4 operates via d_{31} piezoelectric transduction, where the reverse piezoelectric effect instigated by applied electric fields at the input port induces vibration along axes orthogonal to the applied field, and in the same mode as that of Fig. 1; and output current is detected at the output port, where the piezoelectric effect converts strain to charge. As shown in Fig. 4(a), the conventional piezoelectric resonator suffers from a triplet of metal-related losses that include not only the intrinsic material loss of the metal, but also metal-to-resonator interface losses, e.g., due to friction, and resistive loss in the metal, especially as the metal is thinned to reduce its contribution to the first two mechanical mechanisms.

The capacitive-piezo resonator of Fig. 4(b), on the other hand, suffers from none of these metal-derived loss mechanisms. First, the mechanical losses go away as soon as the electrode is separated from the resonator. Second, the electrode can now be made as thick as desired to reduce resistive loss without mechanical loss penalty. Indeed, measured results confirm all of this, with *Q*s as high as high as 3,073 at 1.2-GHz (*cf*. Fig. 5 [17]), and as high as 12,748 at 51-MHz for resonators with good anchor isolation (*cf*. Fig. 6 [18]). These are still not sufficient for RF channel-selection, but they are getting ever closer, and it is known that the AlN film depositions for these devices were not optimum. With optimization, it is not unreasonable to expect capacitive-piezo devices like these to eventually attain *Q* >10,000 at 3GHz, after which boosting by linking higher *Q*, e.g., diamond, resonators might be used to raise *Q*s past 30,000.

Of course, separating the electrodes comes with a penalty in coupling strength. Indeed, if gaps as large as the 6μm of a quartz BVA [19] predecessor were used, the coupling coefficient would be very small, on the order of (C_x/C_o) ~0.014%. With submicron gaps, however, coupling coefficients on the order of those achievable by conventional piezoelectric resonators ensue, and the gaps can actually be quite large by today's standards and still meet the (C_x/C_o) ~0.075% needed for RF channel-selection at 3GHz. Fig. 7 illustrates this with a plot of (C_x/C_o) versus electrode-to-resonator gap spacing for 1.2-GHz versions of Fig. 4's conventional and capacitive-piezo ring devices, with comparison to the RF channel-selection bogey. Note how the capacitive-piezo resonator satisfies the 0.075% requirement even for rather large gaps of 250nm. Of course, higher (C_x/C_o) might be desired for lower R_x, and the capacitive-piezo transducer is clearly capable of this.

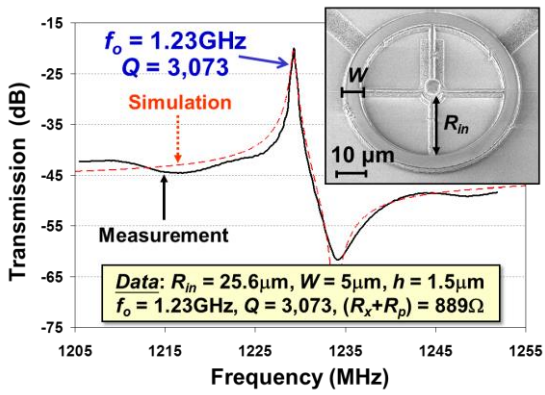

Fig. 5: Measured frequency response for a 1.2-GHz capacitive-piezo 2nd radial-contour mode ring resonator [17].

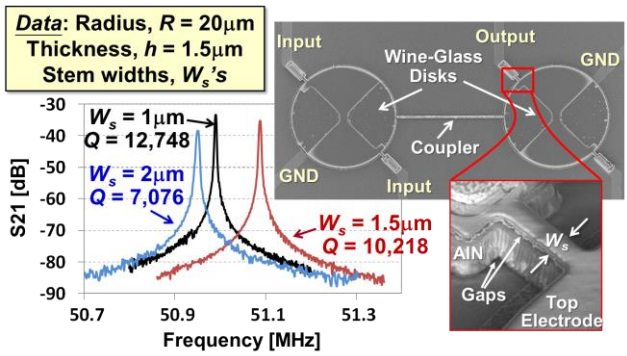

Fig. 6: Measured frequency response for a 51-MHz two-disk array-composite of capacitive-piezo wine-glass disks with varying support beam widths [18].

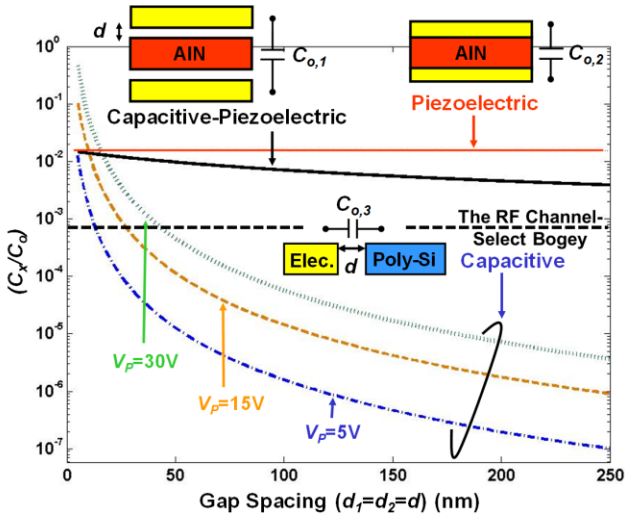

Fig. 7: Comparison of (C_x/C_o) for conventional piezoelectric, capacitive-piezo transducers, and capacitive-gap with V_P of 5V to 30V, all as a function of gap spacing, given the same resonator type and frequency ~1.2 GHz. The RF channel-select bogey for a single filter (without tuning inductor) is also indicated.

Capacitive-Gap Transducers (Revisited)

In addition to predictions for conventional piezoelectric and capacitive-piezo resonators, Fig. 7 plots curves for a capacitive-gap transduced ring using the structure of Fig. 1 under several dc-bias voltages. Interestingly, although the capacitive-gap transduced device is horrid for gaps greater than 100nm, with a (C_x/C_o) ~0.00002% for a 200nm gap and V_P=5V; its values shoot up when the gap is less than 50nm. The rise in (C_x/C_o) with gap spacing actually goes by a third power, as can be seen from the expression

$$\left(\frac{C_x}{C_o}\right) = \frac{2\varepsilon_o}{\pi^2 (m-1)^2 E} \cdot \frac{(r_o - r_i)V_P^2}{d_o^3} \qquad (1)$$

where variables are defined in Fig. 1. From Fig. 7, if there is no limit to gap size, the capacitive-gap transducer ultimately bests the piezoelectric options, and by very large margins for sub-10nm gaps. In this light, the real question when choosing between technologies becomes one of yield. While capacitive-gap transducers can ultimately achieve the highest (C_x/C_o)'s, they require very small electrode-to-resonator gaps to do so, and such gaps may not yield as well as the much larger gaps acceptable for capacitive-piezo transducers. In the end, yield (= cost) may ultimately decide which approach makes the most sense.

From (1), the (C_x/C_o) of a capacitive-gap transduced device also has a strong square-law dependence on the dc-bias voltage V_P. The dc-bias voltage has long been considered a constrained quantity, limited to values below the smallest breakdown voltage of the transistors normally accompanying the MEMS device. However, new technology on the horizon that replaces transistor switches with resonant mechanical ones (a.k.a., resoswitches) with much higher breakdown voltages is now poised to break this voltage limit [20]. Indeed, if this technology can raise voltages to higher than 30V, Fig. 7 shows that the gap needed for RF channel-selection become >50nm, which already yield well in university fabrication facilities.

MICROMECHANICAL POWER GAIN

In addition to charge pumps, higher frequency resoswitches also offer a method for realizing amplification without the need for transistors and their associated quiescent current draws. As described in [21], the resoswitch is similar to a conventional micromechanical resonator, but differs in that it provides displacement gain made possible by both high Q at resonance and structural design, e.g., stiffness engineering using slots and a coupling beam [22]; and its output resonator is designed to actually impact an output electrode during vibration. If the resonator and electrode are constructed in conductive materials, this impacting effectively closes a low loss switch with a very large "off" to "on" transition slope, many times steeper than offered by any semiconductor switch. This means a power supply connected to the output resonator structure, as shown in Fig. 8, can be switched directly to a filter's output electrode at an input FSK frequency, just as occurs in any transistor switch-based gain circuit, but in this case, without quiescent current draw when there is no input signal and with a preceding channel-selecting filter function that removes blockers to allow this degree of amplifier nonlinearity.

The resoswitch device is equally useful when employed on the transmit side. In particular, similar to traditional (non-resonant) RF MEMS switches, the switch figure of merit (FOM_{sw}) for a resoswitch device is on the order of 60THz, which is two orders higher than the 600GHz typical of transistor switches. This should translate to substantially better drain efficiency when a Class E power amplifier employs a resoswitch device instead of

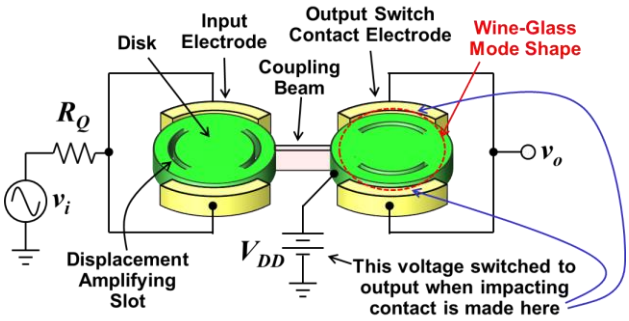

Fig. 8: Perspective-view illustration of a resoswitch filter-amplifier under an appropriate bias and excitation configuration. Here, the mechanically-coupled disks are designed to operate in wine-glass modes and slots are used to effect displacement amplification, where displacement is larger along a slot axis since the stiffness along this axis is smaller than that along the orthogonal axis. This displacement amplification insures that impacting does not occur along the input axis when it occurs along the output switch axis, where it periodically connects the output to V_{DD}, sending its power to the output node, and thus, serving as a power amplifier. The whole structure provides both channel-select filtering and power amplification.

presently used semiconductor switches. Predicted efficiencies are higher than 90%, to be compared with the 65% attained using GaAs transistor switches [23]. This savings in transmit power is especially desirable for sensor networks that use sleep modes to save receive power.

CONCLUSIONS

RF channel-selection enabled by the extremely high *Q*'s >30,000 and massive numbers of MEMS-based resonators stands to be a key enabler for not only software-defined cognitive radio, but also ultra-low power radios for long-lived sensor networks. While these are already groundbreaking possibilities, perhaps, the most compelling and important contribution of this technology is its propensity to encourage wireless designers to break existing assumptions, e.g., that front-end high-*Q* passives must be minimized, and open their minds to the possibility of having *Q*'s >40,000 in abundance, allowing them to use as many high-*Q* passives as they please. Once this happens, an explosion of not only communication architectures, but even also wireless standards, might ensue, and in turn, foster proportional advancements in the capability of our wireless networks. Perhaps, communication hardware and standards designers, alike, should start considering RF channel-selection for their forecasting roadmaps.

But before getting too excited about the possibilities, it is prudent to remind ourselves that much work still remains. Indeed, anything that seems too perfect generally is not perfect, and the frequency-gating spectrum analyzer of Fig. 3 is no exception. Needless to say, there are practical problems that must be overcome, from impedance matching, to frequency repeatability, to frequency stability (e.g., against environmental variations), to integration with control electronics. Vibrant research efforts are already underway to address these issues.

ACKNOWLEDGEMENTS

Much of the work summarized was supported by funding from DARPA.

REFERENCES

[1] T. L. Naing, *et al.*, "2.97-GHz CVD diamond ring resonator with *Q*>40,000," in *Proceedings, IFCS'12*, pp. 570-575.

[2] W.-T. Hsu, "Recent progress in silicon MEMS oscillators," in *Proceedings, PTTI'08*, Reston, Virginia, Dec. 1-4, 2008.

[3] J. L. Hilbert, "RF-MEMS for Wireless Communications," *IEEE Communications Magazine*, pp. 68-74, August 2008.

[4] W.-T. Hsu, *et al.*, "Stiffness-compensated temperature-insensitive …," in *Tech. Digest, MEMS'02,* pp. 731-734.

[5] A. K. Samarao and F. Ayazi, "Temperature compensation of silicon resonators via degenerate doping," *IEEE Trans. on Electron Devices*, vol. 59, no. 1, pp. 87-93, Jan. 2012.

[6] B. Kim, *et al.*, "Frequency stability of … MEMS resonators," in *Digest of Technical Papers, Transducers'05*, Seoul, Korea, June 2005, pp. 1965-1968.

[7] S.-S. Li, *et al.*, "Self-switching vibrating micromechanical filter bank," in *Proceedings, IFCS'05*, 2005, pp. 135-141.

[8] J. Mitola, "The software radio architecture," *IEEE Commun. Mag.*, pp. 26-38, May 1995.

[9] C. T.-C. Nguyen, "MEMS-based RF channel-selection for true software-defined cognitive radio and low power sensor communications," *IEEE Commun. Mag.*, April 2013.

[10] C. T.-C. Nguyen, "Frequency-selective MEMS for … low-power communication devices," *IEEE Trans. Microwave Theory Tech.*, vol. 47, no. 8, pp. 1486-1503, Aug. 1999.

[11] C. T.-C. Nguyen, "Integrated micromechanical RF circuits for software-defined cognitive radio," in *Proc. of the 26th Symposium on Sensors, Micromachines & Applied Systems*, Tokyo, Japan, Oct. 15-16, 2009, pp. 1-5.

[12] S.-S. Li, *et al.*, "An MSI micromechanical differential disk-array filter," in *Tech. Dig., Transducers'07*, pp. 307-311.

[13] M. Rinaldi, *et al.*, "Reconfigurable CMOS oscillator based on multifrequency AlN contour-mode …," *IEEE Trans. Electron Devices*, vol. 58, no. 5, pp. 1281-1286, May 2011.

[14] C.-M. Lin, *et al.*, "AlN/3C–SiC composite plate enabling high-frequency and high-*Q* micromechanical …," *Advanced Materials*, vol. 24, no. 20, pp. 2722-2727, May 2012.

[15] G. R. Kline, *et al.*, "Overmoded high *Q* resonators for microwave …," in *Proceedings, IFCS'93*, pp. 718-721..

[16] L.-W. Hung, *et al.*, "*Q*-boosted AlN array-composite … with *Q* >10,000," in *Tech. Digest, IEDM'10*, pp. 162-165.

[17] L.-W. Hung, *et al.*, "Capacitive-piezo transducers … at 1.2 GHz," *Hilton Head MEMS'10*, pp. 463-466.

[18] L.-W. Hung, *et al.*, "Capacitive-Piezoelectric AlN … with *Q* >12,000," in *Tech. Digest, MEMS'11*, pp. 173-176.

[19] R. J. Besson, *et al.*, "Further advances on B.V.A. quartz resonators," in *Proceeedings, IFCS'80*, pp. 175-182.

[20] Y. Lin, *et al.*, "A micromechanical resonant charge pump," in *Tech. Digest, Transducers'13*, June 16-20, 2013.

[21] Y. Lin, *et al.*, "Metal micromechanical resonant switch for on-chip power applications," in *Tech. Digest, IEEE Int. Electron Devices Mtg.*, Washington, DC, Dec. 5-7, 2011.

[22] B. Kim, *et al.*, "Micromechanical resonant displacement gain stages," in *Tech. Digest, MEMS'09*, pp. 19-22.

[23] C. Meliani, *et al.*, "A 2.4-GHz GaAs-HBT class E MMIC amplifier with 65% PAE," in *Proceedings, IEEE MTT-S IMS'07*, Honolulu, Hawaii, June 3-8, 2007, pp.1087-1090.

CONTACT

*Clark T.-C. Nguyen, ctnguyen@eecs.berkeley.edu.